

# Hysteresis modelling of reinforced concrete columns under pure cyclic torsional loading

Taratal Ghosh Mondal<sup>1</sup>, Sriharsha R. Kothamuthyala<sup>2</sup> and S. Suriya Prakash<sup>\*2</sup>

<sup>1</sup>School of Civil Engineering, Purdue University, United States

<sup>2</sup>Department of Civil Engineering, Indian Institute of Technology Hyderabad, India

(Received May 17, 2017, Revised June 3, 2017, Accepted June 10, 2017)

**Abstract.** It has been observed in the past that, the reinforced concrete (RC) bridge columns are very often subjected to torsional moment in addition to flexure and shear during seismic vibration. Ignoring torsion in the design can trigger unexpected shear failure of the columns (Farhey *et al.* 1993). Performance based seismic design is a popular design philosophy which calls for accurate prediction of the hysteresis behavior of structural elements to ensure safe and economical design under earthquake loading. However, very few investigations in the past focused on the development of analytical models to accurately predict the response of RC members under cyclic torsion. Previously developed hysteresis models are not readily applicable for torsional loading owing to significant pinching and stiffness degradation associated with torsion (Wang *et al.* 2014). The present study proposes an improved polygonal hysteresis model which can accurately predict the hysteretic behavior of RC circular and square columns under torsion. The primary curve is obtained from mechanics based softened truss model for torsion. The proposed model is validated with test data of two circular and two square columns. A good correlation is observed between the predicted and measured torque-twist behavior and dissipated energy.

**Keywords:** polygonal hysteresis model; RC column; torsion; primary curve; unloading and reloading rules

## 1. Introduction

Reinforced concrete (RC) members undergo torsional loading under various conditions (Mondal and Prakash 2015a). Torsion in bridge columns can be induced by skewed or horizontally curved bridges, bridges with outrigger bents and unequal spans or column heights. Therefore, RC columns should be properly designed to dissipate seismic energy adequately through inelastic deformation under vibrations during earthquakes in the presence of torsional loading. Seismic analysis of RC columns requires development of accurate hysteresis model that can predict the stiffness degradation, strength degradation, ductility and damage characteristics of the members under cyclic loading (Prakash 2009, Prakash and Belarbi 2010, Belarbi *et al.* 2010, Goodnight *et al.* 2013). Moreover, understanding the effects of torsion on hysteretic energy dissipation is essential for developing the damage based design approaches for designing new structural elements as well as for determining retrofit solutions for existing elements. Owing to all these reasons it is important to have a proper hysteresis model which can accurately predict the cyclic torsional behavior of RC members considering strength and stiffness degradation along with the pinching effects.

A review of previous studies indicates that, hysteresis modelling approaches adopted by different researchers in

the past are predominantly of two types, namely polygonal hysteresis models (PHMs) and smooth differential models (SDM). In polygonal hysteresis models, the response of an entity is represented by a set of path defining piecewise linear or nonlinear functions. The PHMs are governed by empirical laws derived based on experimental observations representing a certain range of the parameters that influence the behavior under cyclic loading. On the other hand, smooth differential models predict the response of a member to a reversed cyclic loading using set of ordinary differential equations.

In polygonal hysteresis models, the hysteresis response of the structural member is predicted using set of control points and paths defined by piecewise linear or nonlinear functions. The control points are established where the change in slope occurs due to the opening and closing of cracks or due to the pinching effect in the case of cyclic loading. The control points and the rules governing the behavior are established from experimental observations and analyzing the experimental data closely. The response of the member is analyzed and is observed to vary with the selected sectional and geometric parameters, the corresponding trend in variation will be the law that governs the behavior. Polygonal hysteresis model by Clough and Johnston (1966) is well known in literature, which uses bilinear primary curve. The primary curve is the response of the member under monotonic loading which acts as basic envelope or backbone and is essential in close prediction of the cyclic response. The accuracy in predicting the cyclic response depends on the accuracy in prediction of the primary curve. Takeda *et al.* (1970) proposed a tri-linear primary curve by including the

---

\*Corresponding author, Professor  
E-mail: [suriyap@iith.ac.in](mailto:suriyap@iith.ac.in)

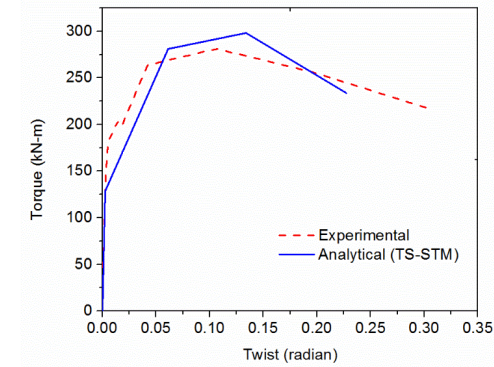
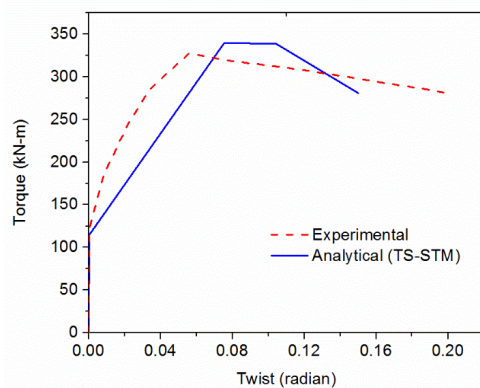
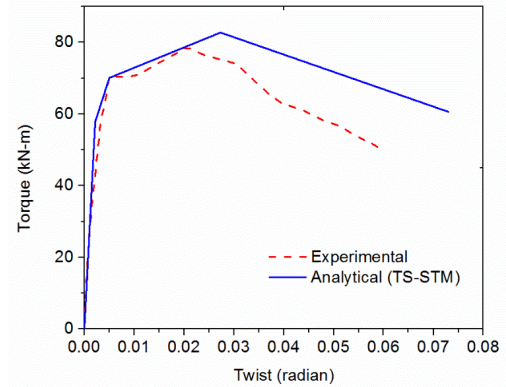
(a) H/D(6)-T/M( $\infty$ )-0.73%(b) H/D(3)-T/M( $\infty$ )-1.32%

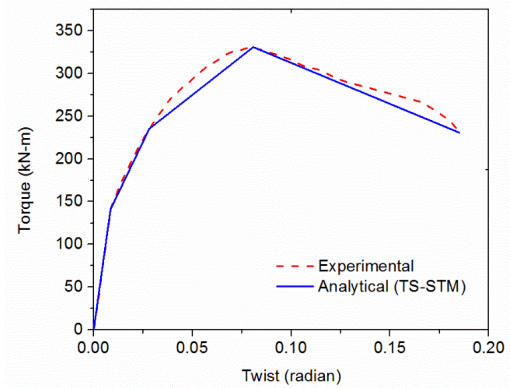
Fig. 1 Primary curves of circular columns under torsion

stiffness change at cracking point in the primary curve and the rules governing the behavior were proposed based on the experimental observations. In the pivot hysteresis model developed by Dowell *et al.* (1998), the envelope curve under monotonic loading had four branches characterizing elastic stiffness, strain hardening, strength degradation and linearly decreasing residual strength. The loading and unloading paths were governed by two pivot points which determine the level of softening with increasing displacement and also the degree of pinching on load reversal. Some other notable works in PHM include Fukada (1969), Aoyama (1971), Atalay and Penzien (1975), Nakata *et al.* (1978), Mansur and Hsu (2005) which were developed from the study of flexure and shear. However, all these models are incapable of predicting the torsional behavior (Wang *et al.* 2014) due to significant pinching, strength and stiffness degradation. Notable work in studying the behavior of structural members under torsion were that of Tirasit and Kawashima (2007), Wang *et al.* (2014). The authors conducted experimental study on behavior of columns under torsion and proposed a semi-empirical approach for predicting the primary curve. In their approach, the yielding torsional moment in the primary curve was calculated using space truss analogy (Rahal and Collins 1995, Mo and Yang 1996) which has its own limitations.

Among all SDMs studied previously, the one proposed by Bouc (1967), Baber and Wen (1981) is most widely used owing to its versatility and robustness. It is also



(a) TP-92



(b) Missouri

Fig. 2 Primary curves of square columns under torsion

computationally efficient and mathematically tractable. The model was subsequently modified by Baber and Noori (1985, 1986) to include the effect of strength and stiffness degradation and pinching and the improved model is popularly known as Bouc-Wen-Baber-Noori (BWBN) model. In the past, Bouc-Wen type models have been used to predict the cyclic response of different structural systems such as, reinforced concrete beams and beam-column joints (Kunnath *et al.* 1997, Sengupta and Li 2013). However, BWBN models have limitations in predicting the torsion dominant behavior which exhibit significant pinching, strength and stiffness degradation.

## 2. Research significance

Only a few investigations in the past have focused on understanding the shear dominant hysteresis behavior including torsion which is the focus of the present investigation. A mechanics based approach using tension stiffened softened truss model previously developed by the authors for circular and square columns (Mondal and Prakash 2015b, 2015c, Ganganagoudar *et al.* 2016a, 2016b) is used for predicting the primary curve. By adopting a more reliable primary curve, torsional hysteresis response can be better predicted. Torsional stiffness reduces drastically after cracking and this important behavior was ignored in the previous models. This stiffness change is accurately captured in the proposed model. Loading and

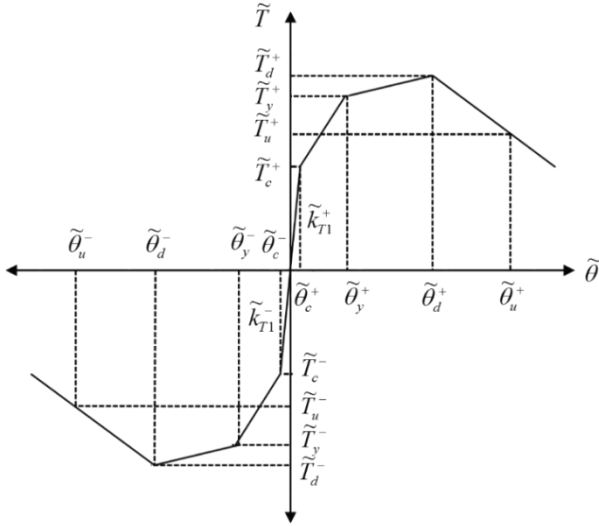


Fig. 3 Idealized primary curve

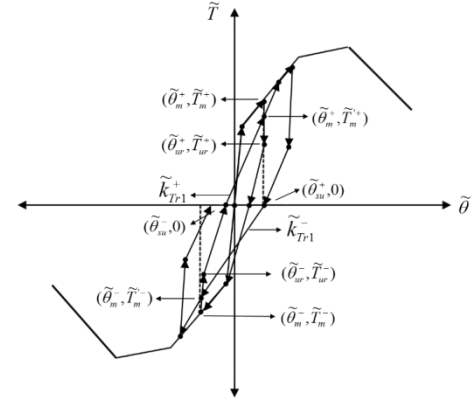
unloading rules for hysteresis behavior is formulated depending upon the trend observed during the statistical analysis of the experimental data. An additional control point has been introduced in the unloading path to capture the pinching behavior more accurately. The comparison of predictions indicates that the proposed model is able to predict the measured experimental behavior closely as explained in the following sections. The proposed model can also be extended to understand the hysteresis behavior under combinations of flexure, shear and torsion loading.

### 3. Experimental corroboration

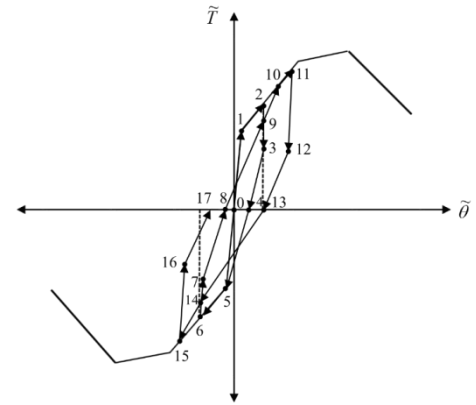
The experimental data of circular and square columns used in this study were tested at University of Missouri Rolla under pure cyclic torsion (Prakash *et al.* 2010). One square column (TP-92) was tested at University of Tokyo (Tirasit and Kawashima 2007). The circular columns had different aspect ratio and percentage of transverse reinforcement. The square column tested at University of Missouri (Prakash *et al.* 2012) had octagonal ties. However, the column tested at University of Tokyo had usual square ties. More details about the experiments can be found elsewhere (Prakash and Belarbi 2009, Tirasit and Kawashima 2007). Due to paucity of test data, development of the proposed model was based on experimental results of limited number of test specimens. Validation of the model for a larger database is a scope of future work.

### 4. Description of hysteresis model

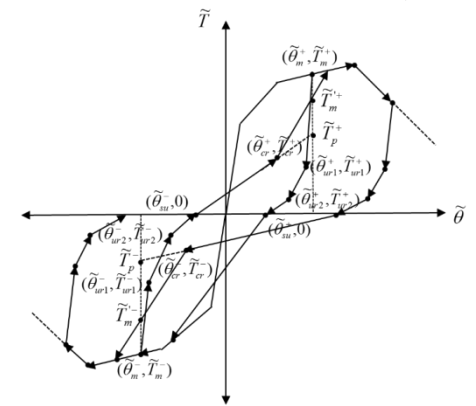
The model consists of a primary envelope curve (Figs. 1-3) and a set of loading and unloading rules (Fig. 4). The control points (Figs. 4(b) and 4(d)) which are estimated by the loading and unloading rules predict the hysteresis loops. Branches that join the successive points are shown in Figs. 4(a) and 4(c). The transition from one control point to another is governed by a set of rules that are determined



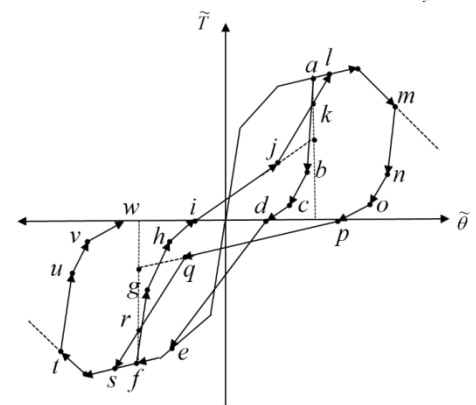
(a) Definition of parameters ( $\tilde{\theta}_c < \tilde{\theta}_m < \tilde{\theta}_y$ )



(b) Hysteresis paths ( $\tilde{\theta}_c < \tilde{\theta}_m < \tilde{\theta}_y$ )



(c) Definition of parameters ( $\tilde{\theta}_m > \tilde{\theta}_y$ )



(d) Hysteresis paths ( $\tilde{\theta}_m > \tilde{\theta}_y$ )

Fig. 4 Characteristics of hysteresis loops

empirically from the experimental data. The details of the model are described in the following sections. Analytical prediction for the primary curves are obtained using tension stiffened-softened truss model (TS-STM) (Mondal and Prakash 2015b, 2015c) developed by the authors.

#### 4.1 Unloading rules

Unloading rules are determined by statistical analysis of experimental data. It was found that the unloading rules are not singular and that they depend on the load reversal point (Fig. 4). Accordingly, separate set of rules were proposed based on the position of the load reversal point on the primary curve. For torsional hysteresis, the unloading rules are mainly governed by physical phenomenon like pinching.

1. The unloading path follows the initial stiffness of the primary curve (path 1→0, 5→0) (Fig. 4) if torsion at the beginning of the unloading is less than the cracking torsion ( $\tilde{T}_m \leq \tilde{T}_c$ ), and  $\tilde{T}_c$  has not been previously exceeded in either direction.

2. After cracking, the unloading path becomes a function of internal variables such as displacement (rotational) ductility ( $\tilde{\theta}_m/\tilde{\theta}_c$  for  $\tilde{\theta}_c < \tilde{\theta}_m < \tilde{\theta}_y$ ,  $\tilde{\theta}_m/\tilde{\theta}_y$  for  $\tilde{\theta}_m > \tilde{\theta}_y$ ) and current deformation level. From a given unloading point on the primary curve ( $\tilde{\theta}_m, \tilde{T}_m$ ), the hysteresis path is directed towards ( $\tilde{\theta}_{ur1}, \tilde{T}_{ur1}$ ) (path 2→3, 6→7, 11→12, 15→16,  $a \rightarrow b$ ,  $f \rightarrow g$ ,  $m \rightarrow n$ ,  $t \rightarrow u$ ) (Fig. 4) which is estimated using the expressions shown in Eq. (1) (Figs. 5, 6, 7, and 8).

a. Circular columns:

$$\frac{\tilde{\theta}_{ur1}}{\tilde{\theta}_m} = -0.0028 \left( \frac{\tilde{\theta}_m}{\tilde{\theta}_c} \right) + 1.0498, \quad \tilde{\theta}_c < \tilde{\theta}_m < \tilde{\theta}_y \quad (1a)$$

$$= -0.0004 \left( \frac{\tilde{\theta}_m}{\tilde{\theta}_y} \right) + 1.0047, \quad \tilde{\theta}_m > \tilde{\theta}_y \quad (1b)$$

$$\frac{\tilde{T}_{ur1}}{\tilde{T}_m} = -0.0009 \left( \frac{\tilde{\theta}_m}{\tilde{\theta}_c} \right) + 0.8527, \quad \tilde{\theta}_c < \tilde{\theta}_m < \tilde{\theta}_y \quad (1c)$$

$$= -0.0006 \left( \frac{\tilde{\theta}_m}{\tilde{\theta}_y} \right) + 0.8623, \quad \tilde{\theta}_m > \tilde{\theta}_y \quad (1d)$$

b. Square columns

$$\frac{\tilde{\theta}_{ur1}}{\tilde{\theta}_m} = -0.0224 \left( \frac{\tilde{\theta}_m}{\tilde{\theta}_c} \right) + 1.0143, \quad \tilde{\theta}_c < \tilde{\theta}_m < \tilde{\theta}_y \quad (1e)$$

$$= 0.0013 \left( \frac{\tilde{\theta}_m}{\tilde{\theta}_c} \right) + 0.931, \quad \tilde{\theta}_m > \tilde{\theta}_y \quad (1f)$$

$$\frac{\tilde{T}_{ur1}}{\tilde{T}_m} = -0.0341 \left( \frac{\tilde{\theta}_m}{\tilde{\theta}_c} \right) + 0.9195, \quad \tilde{\theta}_c < \tilde{\theta}_m < \tilde{\theta}_y \quad (1g)$$

$$= -0.0125 \left( \frac{\tilde{\theta}_m}{\tilde{\theta}_c} \right) + 0.8515, \quad \tilde{\theta}_m > \tilde{\theta}_y \quad (1h)$$

3. In case of unloading beyond the yield point ( $\tilde{\theta}_m > \tilde{\theta}_y$ ), from ( $\tilde{\theta}_{ur1}, \tilde{T}_{ur1}$ ), the unloading path leads to ( $\tilde{\theta}_{ur2}, \tilde{T}_{ur2}$ ) (path  $b \rightarrow c$ ,  $g \rightarrow h$ ,  $n \rightarrow o$ ,  $u \rightarrow v$ ) (Fig. 4), which is given by Eq. (2) (Figs. 9 and 10). However, this branch is non-existent for unloading before the yield point ( $\tilde{\theta}_c < \tilde{\theta}_m < \tilde{\theta}_y$ ).

a. Circular columns:

$$\frac{\tilde{\theta}_{ur2}}{\tilde{\theta}_m} = -0.0363 \left( \frac{\tilde{\theta}_m}{\tilde{\theta}_y} \right) + 0.7101 \quad (2a)$$

$$\frac{\tilde{T}_{ur2}}{\tilde{T}_m} = -0.0126 \left( \frac{\tilde{\theta}_m}{\tilde{\theta}_y} \right) + 0.3243 \quad (2b)$$

b. Square columns:

$$\frac{\tilde{\theta}_{ur2}}{\tilde{\theta}_m} = -0.0141 \left( \frac{\tilde{\theta}_m}{\tilde{\theta}_y} \right) + 0.5065 \quad (2c)$$

$$\frac{\tilde{T}_{ur2}}{\tilde{T}_m} = -0.0097 \left( \frac{\tilde{\theta}_m}{\tilde{\theta}_y} \right) + 0.3121 \quad (2d)$$

4. Next, the hysteresis loop proceeds straight towards ( $\tilde{\theta}_{su}, 0$ ) on the zero load axis (path 3→4, 7→8, 12→13, 16→17,  $c \rightarrow d$ ,  $h \rightarrow i$ ,  $o \rightarrow p$ ,  $v \rightarrow w$ ) (Fig. 4). The reloading point ( $\tilde{\theta}_{su}, 0$ ) can be calculated as shown in Eq. (3) (Figs. 11 and 12). It may be noted here that, at this point there is some residual deformation even though torsional resistance is zero. This can be attributed to the inelastic behavior of the materials.

a. Circular columns:

$$\frac{\tilde{\theta}_{su}}{\tilde{\theta}_m} = -0.0015 \left( \frac{\tilde{\theta}_m}{\tilde{\theta}_c} \right) + 0.2358, \quad \tilde{\theta}_c < \tilde{\theta}_m < \tilde{\theta}_y \quad (3a)$$

$$= 0.1012 \left( \frac{\tilde{\theta}_m}{\tilde{\theta}_y} \right) + 0.0848, \quad \tilde{\theta}_m > \tilde{\theta}_y \quad (3b)$$

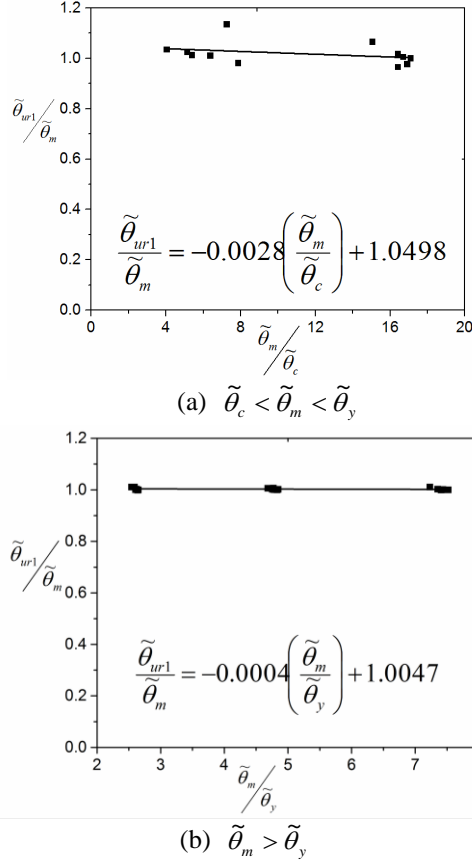
b. Square columns:

$$\frac{\tilde{\theta}_{su}}{\tilde{\theta}_m} = 0.0056 \left( \frac{\tilde{\theta}_m}{\tilde{\theta}_c} \right) + 0.17, \quad \tilde{\theta}_c < \tilde{\theta}_m < \tilde{\theta}_y \quad (3c)$$

$$= 0.0257 \left( \frac{\tilde{\theta}_m}{\tilde{\theta}_y} \right) + 0.1407, \quad \tilde{\theta}_m > \tilde{\theta}_y \quad (3d)$$

#### 4.2 Loading/reloading rules

Loading/reloading rules are another essential component of PHMs which are generally governed by physical


 Fig. 5 Dependence of  $\tilde{\theta}_{ur1}/\tilde{\theta}_m$  on ductility ratio for circular columns

phenomena like strength and stiffness degradation.

1. Initial loading and reloading follow the primary curve (path 1→0, 5→0) (Fig. 4) until the load is reversed at a level higher than the cracking load.
2. After cracking, the first loading in the opposite direction is directed towards the cracking load in the opposite direction (path 4→5) (Fig. 4).
3. When cracking load on both directions has been reached, the reloading path, till yielding, the load path follows a straight line (paths 8→9, 13→14) (Fig. 4) having a slope given by Eq. (4) (Fig. 13) and it extends up to the rotational level from where load was reversed in the previous half-cycle. Since the rotation of the target point is known, and the slope of the branch is also known, therefore, the torsional moment at the target point can be easily computed.

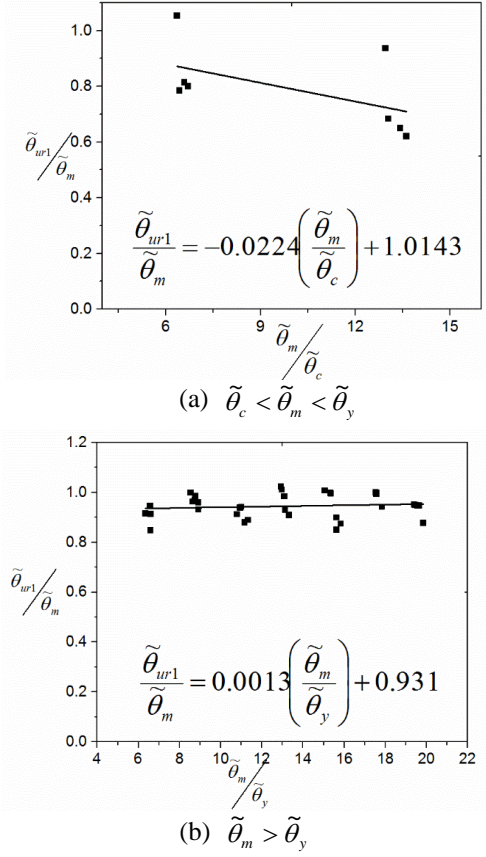
a. Circular columns:

$$\frac{\tilde{K}_{Tr1}}{\tilde{K}_{T1}} = 0.7513 \left( \frac{\tilde{\theta}_m}{\tilde{\theta}_c} \right)^{-0.786} \quad (4a)$$

b. Square columns:

$$\frac{\tilde{K}_{Tr1}}{\tilde{K}_{T1}} = 0.84 \left( \frac{\tilde{\theta}_m}{\tilde{\theta}_c} \right)^{-0.871} \quad (4b)$$

4. After yielding, reloading path up to  $\tilde{\theta}_{cr}$  ( $i \rightarrow j$ ,  $p \rightarrow q$ ) (Fig. 4) follows a straight line passing through  $(\tilde{\theta}_m, \tilde{T}_p)$ .


 Fig. 6 Dependence of  $\tilde{\theta}_{ur1}/\tilde{\theta}_m$  on ductility ratio for square columns

$\tilde{\theta}_{cr}$  can be estimated from Eq. (5a) or Eq. (5c) (Figs. 14(a) and 15(a)) depending upon the shape of the cross-section.  $\tilde{\theta}_m$  is the rotation level from where load was reversed in the previous half-cycle, which is known.  $\tilde{T}_p$  is obtained from the relation shown in Eq. (5b) or, Eq. (5d) (Figs. 14(b) and 15(b)).  $\tilde{T}_{cr}$  can be computed utilizing the knowledge of the values for  $\tilde{\theta}_m$ ,  $\tilde{T}_p$  and  $\tilde{\theta}_{cr}$ .

a. Circular columns:

$$\frac{\tilde{\theta}_{cr}}{\tilde{\theta}_m} = (-0.0067n + 0.0766) \left( \frac{\tilde{\theta}_m}{\tilde{\theta}_y} \right) + (0.0782n + 0.0037) \quad (5a)$$

$$\frac{\tilde{T}_p}{\tilde{T}_m} = (-0.0783n + 0.9425) \left( \frac{\tilde{\theta}_m}{\tilde{\theta}_y} \right)^{(0.1155n - 1.3943)} \leq 1 \quad (5b)$$

b. Square columns:

$$\frac{\tilde{\theta}_{cr}}{\tilde{\theta}_m} = (-0.0039n + 0.0243) \left( \frac{\tilde{\theta}_m}{\tilde{\theta}_y} \right) + (0.0867n - 0.0184) \quad (5c)$$

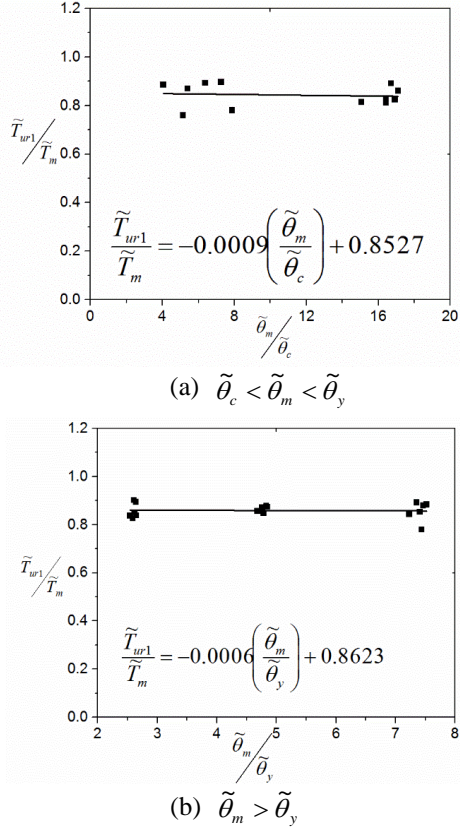


Fig. 7 Dependence of  $\tilde{T}_{ur1}/\tilde{T}_m$  on ductility ratio for circular columns

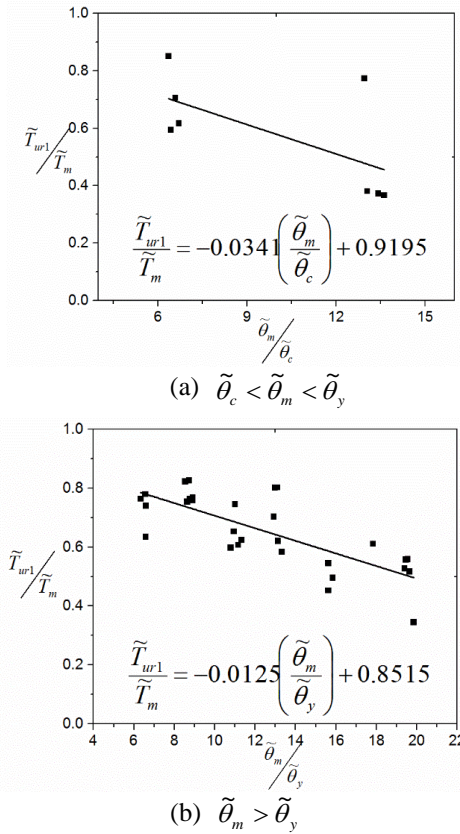


Fig. 8 Dependence of  $\tilde{T}_{ur1}/\tilde{T}_m$  on ductility ratio for square columns

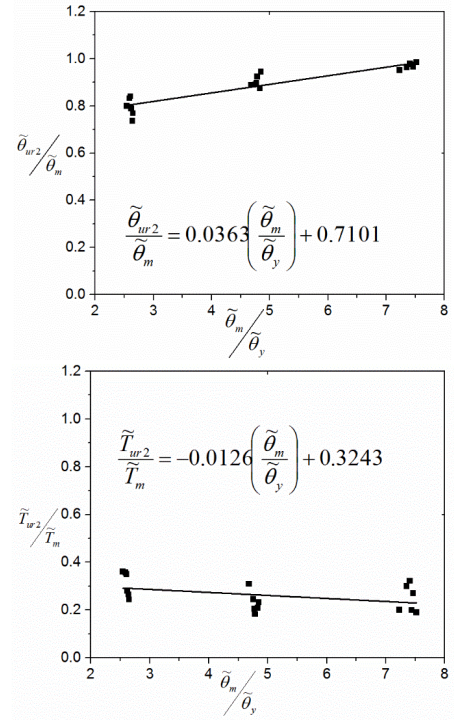


Fig. 9 Dependence of  $\tilde{\theta}_{ur2}/\tilde{\theta}_m$  and  $\tilde{T}_{ur2}/\tilde{T}_m$  on  $\tilde{\theta}_m/\tilde{\theta}_y$  for circular columns

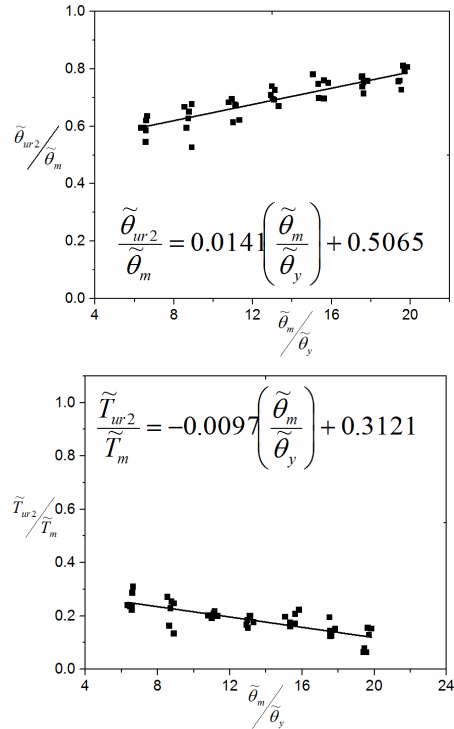
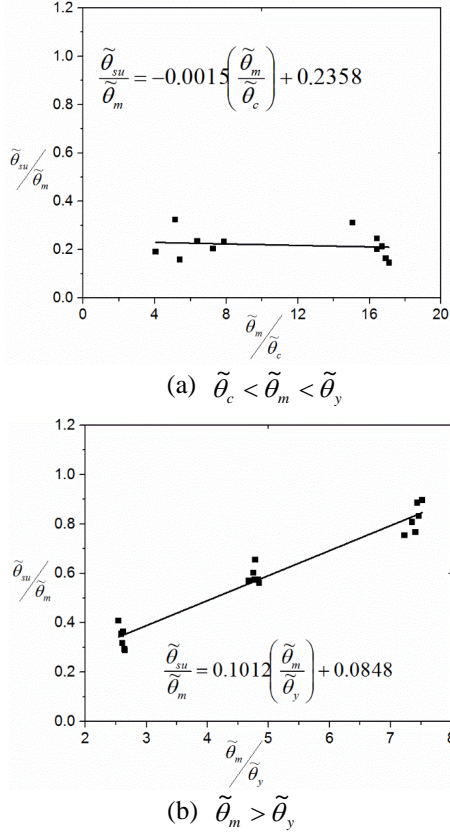


Fig. 10 Dependence of  $\tilde{\theta}_{ur2}/\tilde{\theta}_m$  and  $\tilde{T}_{ur2}/\tilde{T}_m$  on  $\tilde{\theta}_m/\tilde{\theta}_y$  for square columns

$$\frac{\tilde{T}_p}{\tilde{T}_m} = (-0.2616n + 2.4065) \left( \frac{\tilde{\theta}_m}{\tilde{\theta}_y} \right)^{(0.0615n - 0.8597)} \leq 1 \quad (5d)$$


 Fig. 11 Dependence of  $\tilde{\theta}_{su}/\tilde{\theta}_m$  on ductility ratio for circular columns

where,  $n$  is counter, indicating number of cycles repeated at unloading point  $\tilde{\theta}_m$ .  $n$  is assigned a value of 1 when first unloading takes place at a given deformation level ( $\tilde{\theta}_m$ ) and incremented every time the load is reversed from any deformation level falling within the range of  $(1 \pm 0.05)\tilde{\theta}_m$ .  $n$  is computed separately for each direction of loading.

5. A slope change is observed at  $(\tilde{\theta}_{cr}, \tilde{T}_{cr})$  due to full closure of cracks. From this point, the loading path proceeds towards  $(\tilde{\theta}_m, \tilde{T}_m)$  (paths  $j \rightarrow k$ ,  $q \rightarrow r$ ) (Fig. 4).

Calculation of  $\tilde{T}'_m$  is governed by Eq. (6) (Fig. 16).

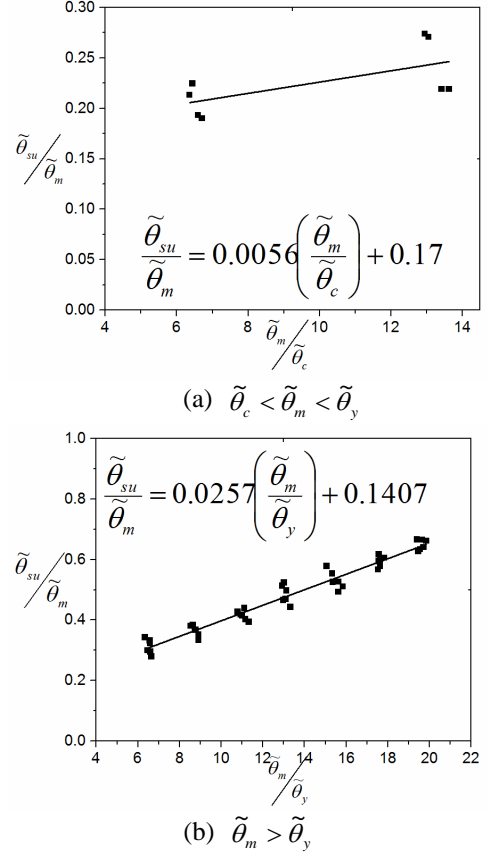
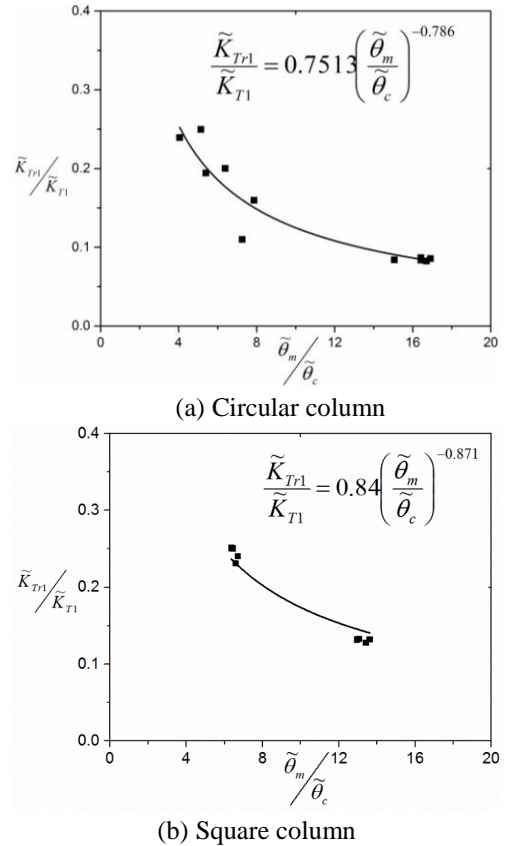
a. Circular Columns:

$$\frac{\tilde{T}'_m}{\tilde{T}_m} = (-0.0557) \left( \frac{\tilde{\theta}_m}{\tilde{\theta}_y} \right) + (0.0177n + 0.9842) \quad (6a)$$

b. Square Columns:

$$\frac{\tilde{T}'_m}{\tilde{T}_m} = (0.0045n - 0.0158) \left( \frac{\tilde{\theta}_m}{\tilde{\theta}_y} \right) + (-0.0132n + 0.9558) \quad (6b)$$

6. Beyond the intersection of reloading branch with primary curve, the loading path follow the primary curve (paths  $l \rightarrow m$ ,  $s \rightarrow t$ ) (Fig. 4). This explains why


 Fig. 12 Dependence of  $\tilde{\theta}_{su}/\tilde{\theta}_m$  on ductility ratio for square columns

 Fig. 13 Dependence of  $\tilde{k}_{Tr1}/\tilde{k}_{T1}$  on  $\tilde{\theta}_m/\tilde{\theta}_c$

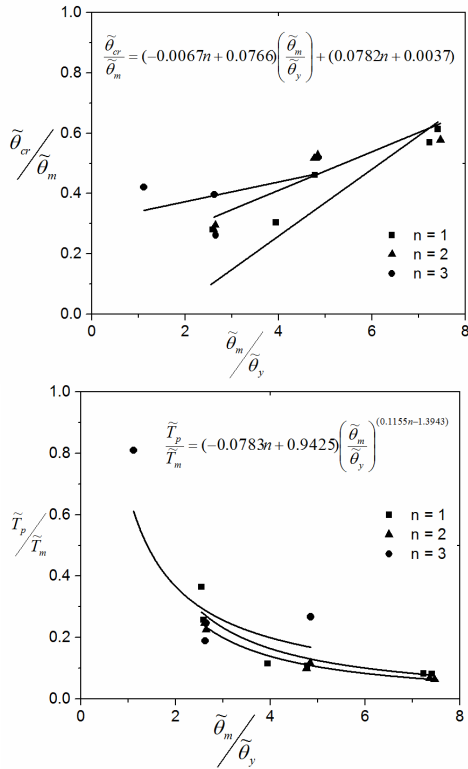


Fig. 14 Dependence of  $\tilde{\theta}_{cr}/\tilde{\theta}_m$  and  $\tilde{T}_p/\tilde{T}_m$  on  $\tilde{\theta}_m/\tilde{\theta}_y$  for circular column

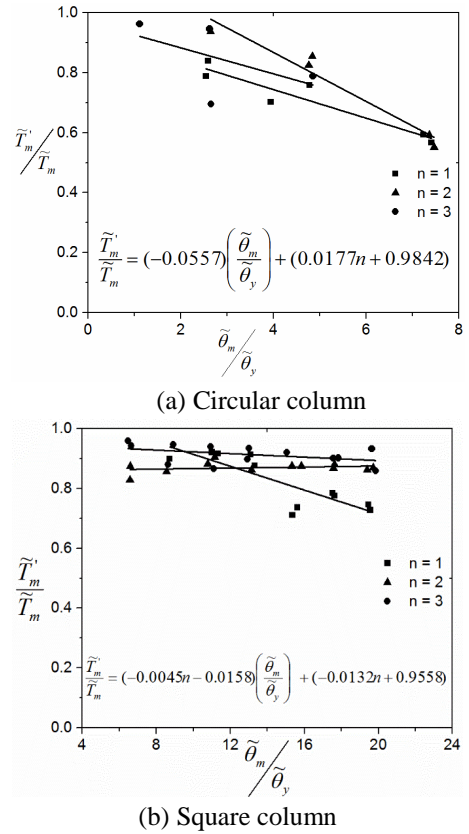


Fig. 16 Dependence of  $\tilde{T}'_m/\tilde{T}_m$  on  $\tilde{\theta}_m/\tilde{\theta}_y$

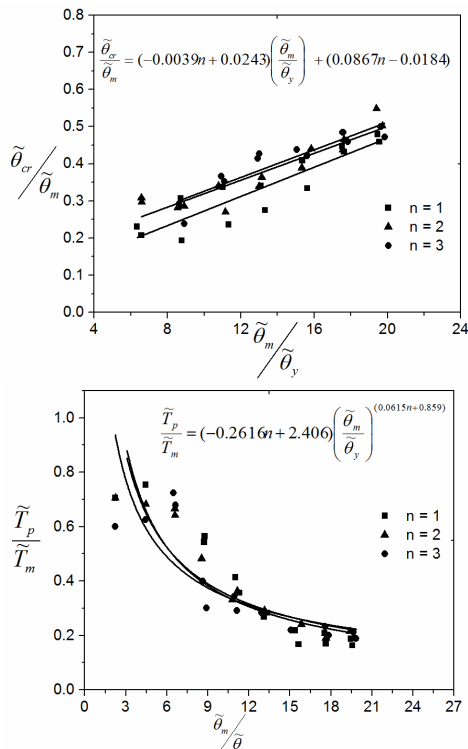


Fig. 15 Dependence of  $\tilde{\theta}_{cr}/\tilde{\theta}_m$  and  $\tilde{T}_p/\tilde{T}_m$  on  $\tilde{\theta}_m/\tilde{\theta}_y$  for square column

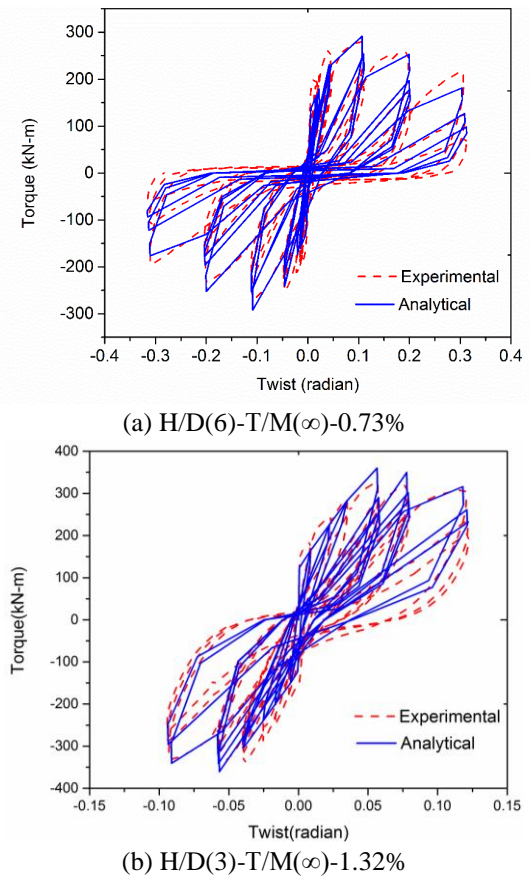


Fig. 17 Prediction of torsional hysteresis of circular columns

accuracy in the prediction of the primary curve greatly influence the accuracy of the estimation of the overall hysteresis behaviour.

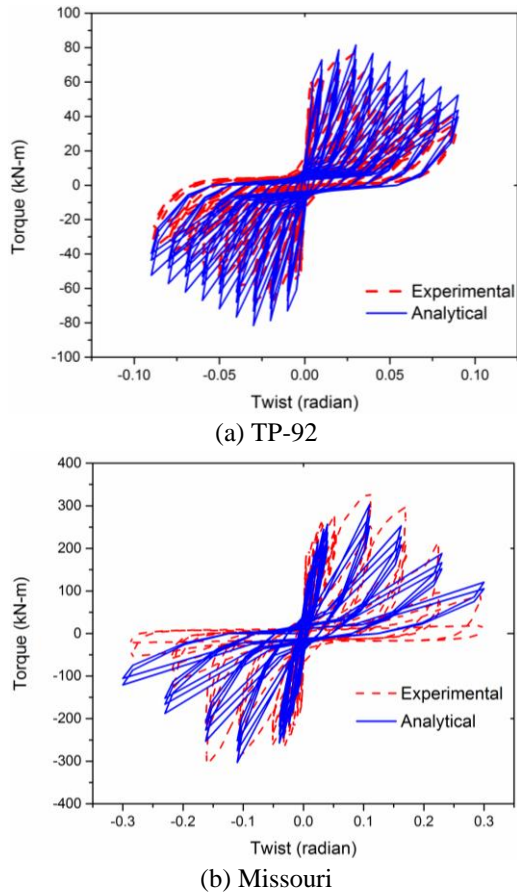


Fig. 18 Prediction of torsional hysteresis of square columns

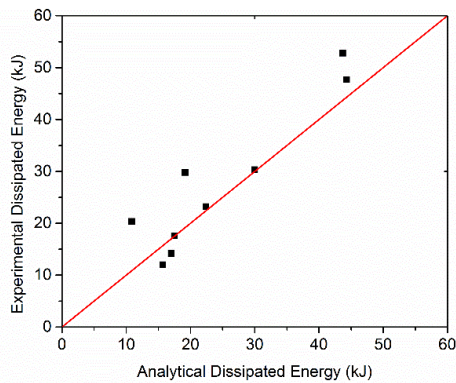
## 5. Results and discussions

### 5.1 Prediction of torque–twist behavior

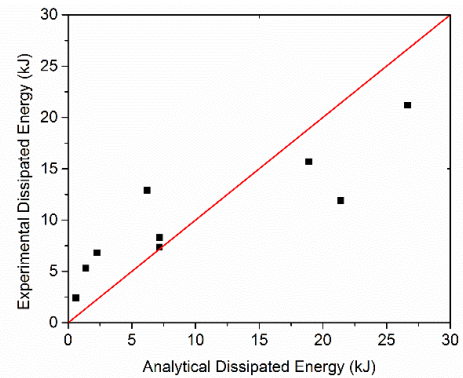
The torque-twist behaviour predicted by the proposed analytical approach is presented and compared with experimental data in Figs. 17 and 18. It is observed that, the model predicted the experimental response of the columns reasonably well. It can also be inferred from the graphs that the model was able to capture complex phenomena like strength and stiffness degradation along with the pinching with reasonable accuracy.

### 5.2 Comparison of dissipated energy

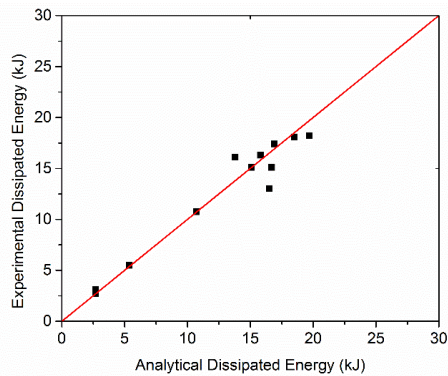
Energy dissipation capacity is one of the most important parameters for damage assessment and health monitoring of reinforced concrete members. The dissipated energy is calculated from the area under the torque twist curves. The comparison of estimated and observed values of dissipated energy for all the columns considered in this study is presented in Fig. 19. Each point in the figures represent energies corresponding to a complete cycle of deformation. The figures show that the proposed analytical model can predict the energy dissipation capacity reinforced concrete columns under torsional moment with reasonable accuracy.



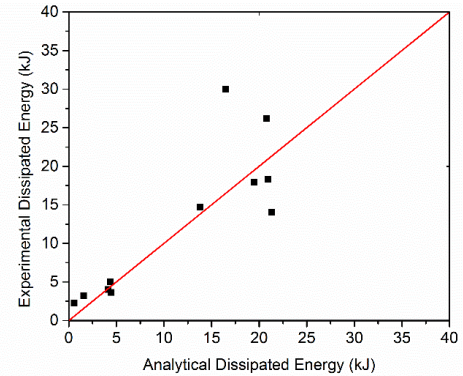
(a) H/D(6)-T/M( $\infty$ )-0.73%



(b) H/D(3)-T/M( $\infty$ )-1.32%



(c) TP-92 Square column



(d) Missouri Square column

Fig. 19 Comparison of experimental and analytical hysteretic energy

## 5. Conclusions

An improved PHM is proposed in this study for reinforced concrete circular and square columns subjected to torsion. The proposed model represents an initial development of a performance based design approach for RC bridge columns under torsional loading. A mechanics based primary curve is used in this study. A slope change has been suggested at the cracking point unlike in the previous models for capturing the behavior more precisely. Unloading and reloading rules are derived based on experimental observations. An additional control point is also introduced in the unloading branch for more accurate prediction of the hysteresis behavior. The predictions of torque-twist behavior showed close correlation with experimental data. Comparison of energy dissipation between square and circular columns of similar sectional details indicate that square columns exhibited lesser energy dissipation due to warping effect when compared to circular columns. The proposed model can be extended in future to predict the hysteretic response of bridge columns under combined loading including torsion. Future studies should also focus on computer implementation of this hysteresis model to realize its utility fully on seismic analysis of bridge systems under torsional loading.

## Acknowledgments

This research was sponsored by SERB, India. Grant number is SB/S3/CEE/0060/2013. The authors gratefully acknowledge their generous support. The authors declare that they have no conflict of interest.

## References

- Aoyama, H. (1971), "Analysis on a school building damaged during the Tockachi-Oki earthquake", *Proceedings of Kanto District Symposium*, Arch. Inst. of Japan, Tokyo, Jan.
- Atalay, M.B. and Penzien, J. (1975), "The seismic behaviour of critical regions of reinforced concrete components influenced by moment, shear and axial force", Report No. UCB/EERC/75/19, University of California, Berkeley.
- Baber, T.T. and Noori, M.N. (1985), "Random vibration of degrading, pinching systems", *J. Eng. Mech.*, **111**(8), 1010-1026.
- Baber, T.T. and Noori, M.N. (1986), "Modeling general hysteresis behavior and random vibration applications", *J. Vib. Acoust. Stress Reliab. Des.*, **108**(4), 411-420.
- Baber, T.T. and Wen, Y.K. (1981), "Random vibration of hysteretic degrading systems", *J. Eng. Mech.*, **107**(6), 1069-1087.
- Belarbi, A., Prakash, S.S. and Silva, P.F. (2010), "Incorporation of decoupled damage index models in the performance-based evaluation of RC circular and square bridge columns under combined loadings", ACI Special Publication-SP271, Vol. 271, 79-102.
- Bouc, R. (1967), "Forced vibration of mechanical systems with hysteresis", *Proceedings of 4<sup>th</sup> conference on Nonlinear Oscillations (extended abstract)*.
- Clough, R.W. and Johnston, S.B. (1966), "Effects of stiffness degradation on earthquake ductility requirements", *Proceedings of the 2<sup>nd</sup> Japan Earthquake Engineering Symposium*, 227-232.
- Dowell, R.K., Seible, F. and Wilson, E.L. (1998), "Pivot hysteresis model for reinforced concrete members", *ACI Struct. J.*, **95**(5), 607-617.
- Farhey, D.N., Adin, M.A. and Yankelevsky, D.Z. (1993), "RC flat slab-column subassemblages under lateral loading", *J. Struct. Eng.*, **119**(6), 1903-1916.
- Fukada, Y. (1969), "A study on the restoring force characteristics of reinforced concrete buildings", *Proceedings of Kanto District Symposium*, Arch. Inst. of Japan, Tokyo, Japan, No. 40. (in Japanese)
- Ganganagoudar, A.G., Mondal, T.G. and Prakash, S.S. (2016a), "Analytical and finite element studies on behaviour of FRP strengthened beams under torsion", *Compos. Struct. J.*, **153**, 876-885.
- Ganganagoudar, A.G., Mondal, T.G. and Prakash, S.S. (2016b), "Improved softened membrane model for reinforced concrete circular bridge columns under torsion", *J. Bridge Eng.*, ASCE, **21**(7), 04016037.
- Goodnight, J., Kowalsky, M. and Nau, J. (2013), "Effect of load history on performance limit states of circular bridge columns", *J. Bridge Eng.*, ASCE, **18**(12), 1383-1396.
- Kunnath, S.K., Mander, J.B. and Fang, L. (1997), "Parameter identification for degrading and pinched hysteretic structural concrete systems", *Eng. Struct.*, **19**(3), 224-232.
- Mansour, M. and Hsu, T. (2005), "Behaviour of reinforced concrete elements under cyclic shear. I: Experiments", *J. Struct. Eng.*, ASCE, **131**(1), 44-53.
- Mo, Y.L. and Yang, R.Y. (1996), "Response of reinforced/prestressed concrete box structures to dynamically applied torsion", *Nucl. Eng. Des.*, **165**(1), 25-41.
- Mondal, T.G. and Prakash, S.S. (2015a), "Nonlinear finite element analysis of RC bridge columns under torsion with and without axial compression", *J. Bridge Eng.*, **21**(2), 04015037.
- Mondal, T.G. and Prakash, S.S. (2015b), "Effect of tension stiffening on the behaviour of reinforced concrete circular columns under torsion", *Eng. Struct.*, **92**(1), 186-195.
- Mondal, T.G. and Prakash, S.S. (2015c), "Effect of tension stiffening on the behaviour of square RC columns under torsion", *Struct. Eng. Mech.*, **54**(3), 501-520.
- Nakata, S., Sproul, T. and Penzien, J. (1978), "Mathematical modeling of hysteresis loops for reinforced concrete columns", Report No. UCB/EERC/78/11, University of California, Berkeley, California.
- Prakash, S., Belarbi, A. and You, Y.M. (2010), "Seismic performance of circular RC columns subjected to axial force, bending, and torsion with low and moderate shear", *Eng. Struct.*, **32**(1), 46-59.
- Prakash, S.S. (2009), "Seismic behavior of RC circular columns under combined loading including torsion.", PhD Thesis, Thesis number: T 9562, Department of Civil Engineering, Missouri University of Science and Technology, Missouri, USA.
- Prakash, S.S. and Belarbi, A. (2009), "Bending-shear-torsion interaction features of RC circular bridge columns-An experimental study", Special Publication-SP265, Vol. 265, 427-454.
- Prakash, S.S. and Belarbi, A. (2010), "Towards damage-based design approach for RC bridge columns under combined loadings using damage index models", *J. Earthq. Eng.*, **14**(3), 363-389.
- Prakash, S.S., Li, Q. and Belarbi, A. (2012), "Behaviour of circular and square RC bridge columns under combined loading including torsion", *ACI Struct. J.*, **109**(3), 317.
- Rahal, K.L. and Collins, M.P. (1995), "Analysis of sections subjected to combined shear and torsion-a theoretical model", *ACI Struct. J.*, **92**, 459-459.
- Sengupta, P. and Li, B. (2013), "Modified Bouc-Wen model for hysteresis behavior of RC beam-column joints with limited

- transverse reinforcement”, *Eng. Struct.*, **46**, 392-406.
- Takeda, T., Sozen, M.A. and Nielsen, N.N. (1970), “Reinforced concrete response to simulated earthquakes”, *J. Struct. Div.*, ASCE, **96**, 2557-2573.
- Tirasit, P. and Kawashima, K. (2007), “Seismic performance of square reinforced concrete columns under combined cyclic flexural and torsional loadings”, *J. Earthq. Eng.*, **11**, 425-452.
- Wang, P., Han, Q. and Du, X. (2014), “Seismic performance of circular RC bridge columns with flexure-torsion interaction”, *Soil Dyn. Earthq. Eng.*, **66**, 13-30.

PL

## Notations

- $\theta_c$  : Twist at cracking point on the primary curve.
- $\theta_y$  : Twist at yield point on the primary curve.
- $\theta_d$  : Twist at the peak on the primary curve.
- $\theta_u$  : Twist at the point where ultimate failure occurs in the primary Curve.
- $\theta_m$  : Twist at the point from where load is reversed.
- $\theta_{ur1}$  : Twist at first control point on the unloading path.
- $\theta_{ur2}$  : Twist at second control point on the unloading path.
- $\theta_{su}$  : Twist on  $\theta$  axis where unloading ends and reloading starts.
- $\theta_{cr}$  : Twist where slope changes while reloading.
- $\tilde{T}_c$  : Torque at cracking point on the primary curve.
- $\tilde{T}_y$  : Torque at yield point on the primary curve.
- $\tilde{T}_d$  : Peak torque on the primary curve.
- $\tilde{T}_u$  : Torque at point where ultimate failure occurs on the primary curve.
- $\tilde{T}_{ur1}$  : Torque at first control point on the unloading path.
- $\tilde{T}_{ur2}$  : Torque at second control point on the unloading path.
- $\tilde{T}_m$  : Reduced strength attained while reloading at the point from where load was reversed.
- $K_{Tr1}$  : Reloading stiffness for  $\tilde{\theta}_c < \tilde{\theta}_m < \tilde{\theta}_y$
- $K_{Tr}$  : Initial pre-crack stiffness of the primary curve.